

# Distribution characteristics of summer precipitation raindrop spectrum in Qinghai–Tibet Plateau

Fuzeng Wang<sup>1,2</sup>, Yuanyu Duan<sup>1</sup>, Yao Huo<sup>1</sup>, Yaxi Cao<sup>1</sup>, Qiusong Wang<sup>1</sup>, Tong Zhang<sup>2</sup>,  
Junqing Liu<sup>3</sup>, Guangmin Cao<sup>4</sup>

<sup>1</sup>College of Electronic Engineering, Chengdu University of Information Technology, Chengdu 610225,  
China

<sup>2</sup>Key Laboratory of Land Surface Process and Climate Change in Cold and Arid Regions, Chinese  
Academy of Sciences, Lanzhou 730000, China

<sup>3</sup>Weather Modification Center for Tibet, Lhasa 850000, China

<sup>4</sup>Heilongjiang Meteorological Data center, Harbin 150000, China

Correspondence to: Guangmin Cao(cgcm909@163.com)

**Abstract:** To enhance the precision of precipitation forecasting in the Qinghai–Tibet Plateau region, a comprehensive study of both macro– and micro–characteristics of local precipitation is imperative. In this study, we investigated the particle size distribution, droplet velocity, droplet number density,  $Z$  (Radar reflectivity) –  $I$  (Rainfall intensity) relationship, and Gamma distribution of precipitation droplet spectra with a single precipitation duration of at least 20 minutes and precipitation of 5 mm or more at four stations (Nyalam, Lhasa, Shigatse, and Naqu) in Tibet during the recent years from June to August. The results are as follows: (1) In the fitting relationship curve between precipitation raindrop spectral particle size and terminal speed at the four stations in Tibet, when the particle size was less than 1.5 mm, the four lines essentially coincided. When the particle size exceeded 1.5 mm, the speed in Nyalam was the highest, followed by Naqu, and the speed in Lhasa was the lowest. The terminal speed of particles correlated with altitude. (2) The six microphysical characteristics( mean diameter ( $D_m$ ), average volume diameter ( $D_v$ ), mode diameter ( $D_d$ ), dominant diameter ( $D_p$ ), and median diameter ( $D_{nd}$ )) at the four stations have different correlation relationships with altitude under different rainfall intensities.  $D_m$  exhibits a negative correlation with altitude at the same rainfall intensity; in contrast,  $D_v$  shows a positive correlation with altitude. For microphysical parameters such as  $D_d$  and  $D_p$ , a rainfall intensity of  $10 \text{ mm}\cdot\text{h}^{-1}$  serves as the boundary line, and they have different correlation relationships with altitude under the same rainfall intensity level. (3) The  $Z$ – $I$  relationships at the four stations exhibited variations. Owing to the proximity in altitude between Lhasa and Shigatse, as well as

删除[远愚 段]: falling

删除[远愚 段]: Shigatse

删除[远愚 段]: Lhasa

删除[远愚 段]: Naqu

删除[远愚 段]: falling

删除[远愚 段]: The diameter of the six microphysical features at the four stations increased with altitude.

30 between Nyalam and Nagqu, the coefficients  $a$  and index  $b$  in the  $Z-I$  relationships of the two groups  
31 of sites were relatively similar. (4) The fitting curves of the Exponential and Gamma distributions of  
32 the precipitation particle size at the aforementioned four stations are largely comparable. The  
33 Exponential distribution fitting exhibits a slightly better effect. The parameter  $\mu$  in Gamma distribution  
34 decreases with the increase of altitude, while  $N_0$  and  $\lambda$  in Exponential distribution show a clear  
35 upward trend with altitude.

删除[远愚 段]: M-P

删除[远愚 段]: M-P

删除[远愚 段]: M-P

## 36 1. Introduction

37 The microphysical processes of cloud and precipitation over the Qinghai-Tibet Plateau significantly  
38 differ from those in low-altitude regions due to the high average altitude and complex, changeable  
39 terrain, resulting in a strong ground heating effect. Due to the terrain's influence, the plateau area has a  
40 limited number of observation stations, leading to a scarcity of precipitation records. Based on three  
41 atmospheric scientific experiments conducted over the Qinghai-Tibet Plateau, convective clouds  
42 exhibit high activity, although the precipitation intensity is moderate(Li et al., 2014; Jiang et al., 2002;  
43 Xu et al., 2006; Li et al., 2001). In the central part of the Plateau, convective clouds constitute 4% to  
44 21%, with cumulonimbus clouds representing 21%. Additionally, the frequency of severe weather, such  
45 as thunderstorms and hail, surpasses that in other regions. In the majority of Qinghai-Tibet Plateau  
46 areas, convective cloud precipitation constitutes over 90% of the total (Chang and Guo, 2016).  
47 Particularly during the rainy season, convective processes are frequent with smaller horizontal scales,  
48 weaker intensities, and shorter durations. Due to observational constraints, short-term tests and satellite  
49 data (e.g., TRMM, CloudSat, and Aqua) are employed to investigate Tibetan Plateau precipitation, with  
50 a focus on liquid precipitation characteristics, including seasonal and diurnal variations and convective  
51 activity's liquid drop spectrum inversion(Ruan et al., 2015; Liu et al., 2015; Xiong et al., 2019; Zhang  
52 et al., 2018). The scarcity of observational data on cloud precipitation's physical processes in the  
53 Qinghai-Tibet Plateau results in limited studies on microscopic parameters' characteristics. The recent  
54 installation of a laser raindrop spectrometer enables a comprehensive understanding of the plateau's  
55 precipitation microphysical parameters through the study of raindrop spectral parameters and  
56 distribution characteristics in various regions.  
57 Some studies have explored the spectral characteristics of raindrops over the Tibetan Plateau. Yu Jianyu

删除[远愚 段]: severe

58 et al. and Shu Lei et al. conducted analyses on the raindrop spectrum characteristics of various clouds  
59 in the Naqu and Yushu regions of the Qinghai–Tibet Plateau(Yu et al., 2020; Shu et al., 2021). Li  
60 Shanshan et al. investigated raindrop spectral characteristics at different elevations on the eastern slope  
61 of the Qinghai–Tibet Plateau. They discovered that the average spectrum of raindrop number  
62 concentration at various elevations conforms to the Gamma function distribution. Moreover, light  
63 precipitation and heavy precipitation exhibit distinct raindrop spectral characteristics(Li et al., 2020).  
64 The aforementioned research was conducted in Naqu and Yushu areas in the Qinghai–Tibet Plateau, as  
65 well as the west Sichuan Plateau area. However, there is a limited number of studies on the spectral  
66 characteristics and distribution rules of cloud precipitation raindrops in various regions of the Tibetan  
67 Plateau. The analysis of raindrop spectrum characteristics in the Naqu region, as mentioned earlier, was  
68 conducted only during the summer months from June to August 2014. In this study, we used raindrop  
69 spectrum data from the Naqu region spanning 2017 to 2020, building upon and extending previous  
70 research. We analyzed the temporal variation of the raindrop spectrum in convective cloud precipitation  
71 across various regions and examined differences in raindrop spectra among these regions. We  
72 conducted a systematic analysis of raindrop spectrum data associated with moderate rain from four  
73 stations with varying altitudes, longitudes, and latitudes. We compared and analyzed the differences in  
74 drop spectrum characteristics among these four stations, which is of great significance for enhancing  
75 the scientific understanding of precipitation's influence in the plateau region.

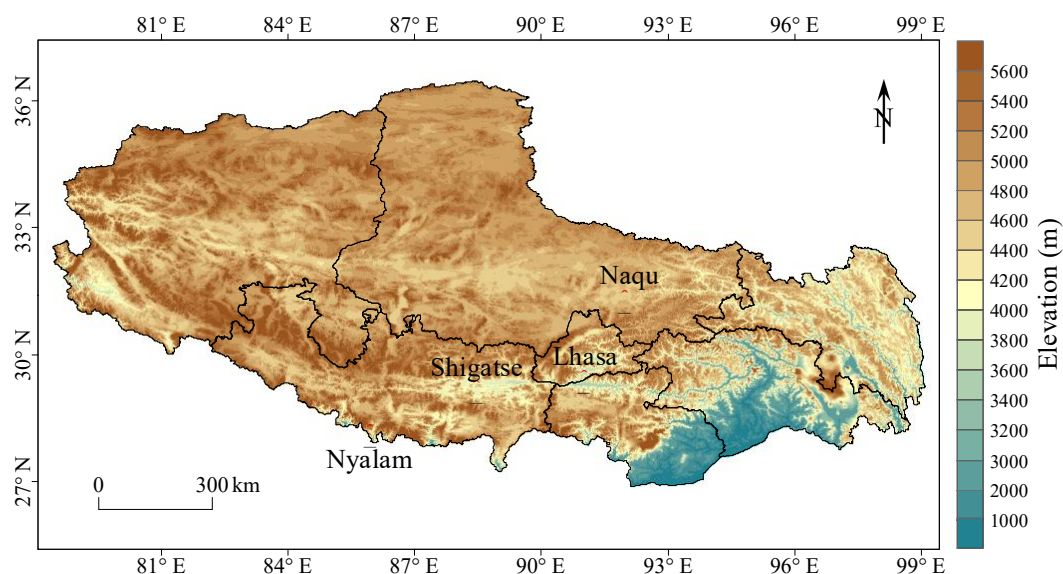
76 The objective of this study is to enhance the understanding of raindrop spectrum characteristics at  
77 various elevations of the Tibetan Plateau. The findings of this study will establish a foundation for  
78 comprehending precipitation characteristics and improving precipitation forecasts at diverse elevations  
79 of the Tibetan Plateau. This study is structured as follows: Data sources and research methods are  
80 described in Section 2. The analysis results are presented in Section 3 while the conclusion and  
81 discussion are provided in Section 4.

## 82 **2. Data and methods**

### 83 **2.1. Data collection**

84 The data obtained for this study consist of raindrop spectrum data from four meteorological stations  
85 (i.e., Nyalam, Lhasa, Shigatse, and Naqu) in Tibet. Owing to its unique climate environment, snowfall

86 occurs time to time from September to May. Data from June to August is selected to analyze the  
 87 precipitation raindrop spectrum process in this study. The precipitation data selection criteria include a  
 88 precipitation process duration exceeding 20 minutes and a single precipitation process with rainfall  
 89 greater than 5mm. As the frequency of convective clouds in most areas of the Qinghai–Tibet Plateau  
 90 exceeds 90%, all collected samples are categorized as convective clouds in this paper. Table 1 displays  
 91 the longitude, latitude, altitude, and sample numbers of the four stations. Figure 1 illustrates the  
 92 geographical distribution of the four sites. The four stations cover a broad area of central Tibet from  
 93 south to north, making the results representative.



94  
 95 **Figure 1: Station distribution and the surrounding terrain**

96 **Table 1: Coordinates, elevation, sampling periods, and sample sizes of the four sites.**

Station	Longitude	Latitude	Elevation	Sampling period	Sample size
Nyalam	85.58° E	28.11° N	4519 m	2017–2019	11579
Lhasa	91.08° E	29.40° N	3653 m	2017–2018	8364
Shigatse	88.53° E	29.15° N	3910 m	2017–2018	14237
Naqu	92.04° E	31.29° N	4560 m	2017–2020	5630

97 **2.2. Quality Control and Quality Assurance (QA/QC)**

98 The Parsivel2 raindrop spectrometer features 32 particle size measurement channels and 32 particle  
 99 velocity measurement channels. The particle size measurement range is 0.062–24.5 mm, and the  
 100 particle velocity measurement range is 0.05–20.8 m s<sup>-1</sup>, with a sampling time of 60 s. In comparison to  
 101 the previous Parsivel raindrop spectrometer model, the Parsivel2 raindrop spectrometer utilizes infrared

102 light as its light source. This change reduces the interference of visible light, resulting in significant  
103 advancements in the measurement of raindrop size and rainfall. Following the sampling principle of the  
104 raindrop spectrometer, the instrument records the particle size and particle speed of all particles passing  
105 through the sampling surface. To mitigate the influence of sand and dust particles, it is imperative to  
106 control the quality of the fundamental data.

107 Atlas(Atlas et al., 1973) discovered a relationship between the terminal velocity of particles and the  
108 particle diameter. In an ideal windless environment, the formula for the terminal velocity of particles is:

删除[远愚 段]: falling

删除[远愚 段]: falling

$$\begin{cases} v=0, & x<0.03 \\ v = 4.323 \times (x - 0.03), & 0.03 \leq x \leq 0.6 \\ v = 9.65 - 10.3 \times e^{-0.6x}, & x > 0.6 \end{cases} \quad (1)$$

109  
110 where  $x$  represents the particle diameter in mm, and  $v$  represents the terminal velocity of the particle  
111 in  $\text{m s}^{-1}$ . Equation (1) is applicable near the ground. For other altitudes, considering the known effect of  
112 atmospheric air density on the terminal terminal velocity, a correction factor for the terminal velocity of  
113 raindrops, accounting for air density, as given by Atlas et al. (1973) and Foote and du Toit et al. (1969),  
114  $(\rho_0/\rho)^{0.4}$  is multiplied on the right-hand side of Equation (1). Here,  $\rho$  is the air density at the observation  
115 altitude, and  $\rho_0$  is the air density at sea level under standard atmospheric pressure.

删除[远愚 段]: falling

116 Kruger and Krajewski(Kruger and Krajewski, 2002) proposed a method to mitigate the dispersion of  
117 velocity over large samples, building on the study by Atlas. Initially, the terminal velocity was  
118 calculated based on the particle diameter and final velocity formula, and subsequently, a threshold  
119 value was set for elimination. The formula is expressed in Equation 2.

$$|v_{measured} - v_A| < 0.4v_A \quad (2)$$

120  
121 where  $v_{measured}$  represents the final velocity measured by the raindrop spectrometer, and  $v_A$  is the final  
122 velocity calculated using the final velocity formula. If the relative error falls within the specified  
123 threshold range, the data will be retained.

124 Previous studies have highlighted that the distribution of raindrop spectra exhibit distinct  
125 characteristics influenced by geographical environment and topography. Hence, utilizing the same  
126 calculation formula across different areas for raindrop spectrum elimination is likely to introduce  
127 significant errors. Therefore, we utilized historical data from a raindrop spectrum site to localize the  
128 parameters identified in the study by Atlas and incorporates them into the formula for particle  
129 elimination. Simultaneously, due to deformation occurring in raindrops during descent, the raindrop

删除[远愚 段]: spectrum

130 spectrum data undergoes distortion and correction after quality control.

### 131 2.3. Raindrop spectrum parameters

132 The number density of the precipitation raindrop spectrum is defined as the total number of particles  
133 per unit volume(Shi et al., 2008).

$$134 \quad N(D) = \sum_{i=1}^{32} \sum_{j=1}^{32} \frac{n_{ij}}{A \cdot \Delta T \cdot V_j} \quad (3)$$

135 where  $N(D)$  is the number density parameter, in units of  $\text{mm}^{-1} \text{m}^{-3}$ ;  $n_{ij}$  represents the number of  
136 raindrops with the diameter of the  $i$ -th particle and the velocity of the  $j$ -th particle;  $A$  is the sampling  
137 base area of the raindrop spectrometer ( $5400 \text{ mm}^2$ );  $\Delta T$  is the sampling time ( $60 \text{ s}$ );  $V_j$  is the velocity  
138 value of the sampled particle, in units of  $\text{m s}^{-1}$ .

139 The average diameter is calculated as the sum of the diameters of all raindrops per unit volume divided  
140 by the total number of raindrops, and the formula is given by equation 4.

$$141 \quad D_l = \frac{\sum_{i=1}^{32} N(D_i) D_i}{\sum_{i=1}^{32} N(D_i)} \quad (4)$$

142 The weighted average diameter represents the average diameter of the weighted mass of all particles  
143 per unit volume relative to the total mass of particles, measured in mm. The formula is expressed in  
144 equation 5.

$$145 \quad D_m = \frac{\sum_{i=1}^{32} N(D_i) D_i^4}{\sum_{i=1}^{32} N(D_i) D_i^3} \quad (5)$$

146 where  $D_i$  represents the diameter of the  $i$ -th particle, and  $N(D_i)$  represents the particle number density  
147 of the  $i$ -th particle diameter.

148 Precipitation intensity refers to precipitation per unit time (per hour), measured in  $\text{mm h}^{-1}$ . The  
149 formula is given by equation 6.

$$150 \quad I = \frac{6\pi}{10^4} \sum_{i=1}^{32} D_i^3 V(D_i) N(D_i) \quad (6)$$

151 The radar reflectivity factor is the sum of the backscattering area of all particles per unit volume,

152 measured in  $\text{mm}^{-6} \text{m}^{-3}$ . The formula is expressed in equation 7.

$$Z = \sum_{i=1}^{32} N(D_i) D_i^6 \quad (7)$$

154 The observed raindrop spectrum is discrete, and the double parameter index, namely ~~Exponential~~ | 删除[远愚 段]: M-P  
155 distribution, can be used to simulate the raindrop particle size distribution(Marshall and Palmer, 1948).

156 The formula is given by equation 8.

$$N(D) = N_0 \times \exp(-\lambda D) \quad (8)$$

158 where  $N_0$  is a number density parameter, measured in  $\text{mm}^{-1} \text{m}^{-3}$ .  $\lambda$  is a size parameter, measured in  
159  $\text{mm}^{-1}$ .

160 However, this distribution pattern has some errors compared with actual observation data when  
161 describing small and large raindrops. Therefore, Ulbrich and Atlas proposed a modified raindrop  
162 particle size distribution pattern. They treated the raindrop spectrum distribution as a Gamma  
163 distribution to correct the distribution pattern between small and large raindrops.

164 In this case, the raindrop particle size distribution follows the Gamma distribution with three  
165 parameters(Carlton and David, 1984). The formula is given by equation 9.

$$N(D) = N_0 \times D^\mu \times \exp(-\lambda D) \quad (9)$$

167 where  $\mu$  is a dimensionless parameter referred to as the shape factor. When  $\mu$  is greater than 0, the  
168 curve exhibits an upward curvature; when  $\mu$  is less than 0, the curve displays a downward curvature.

169 When  $\mu=0$ , it corresponds to an ~~Exponential~~ distribution. | 删除[远愚 段]: M-P

170 Zhang(Zhang et al., 2003) pointed out a binomial relationship between  $\mu$  and  $\lambda$  when studying the  $\mu$ - $\lambda$   
171 relationship of precipitation in Florida:

$$\lambda = a\mu^2 + b\mu + c \quad (10)$$

173 Ulbrich(Ulbrich, 1983) pointed out in his study that the  $\mu$ - $\lambda$  relation under Gamma distribution can be  
174 expressed as:

$$D_m = \frac{4+\mu}{\lambda} \quad (11)$$

176 Equation (11) shows that there is a relationship between the ratio of  $\mu$  and  $\lambda$  and the weighted average  
177 diameter of mass. The Gamma distribution fit is typically applied to the observed raindrops distribution  
178  $N(D)$  using the least squares or order moments method. In this study, the least square method is

179 employed to fit the Exponential and Gamma distributions.

删除[远愚 段]: M-P

### 180 3. Result and discussion

181 The average altitude of the Qinghai-Tibet Plateau is over 4000 m, and the terrain is complex and  
182 changeable, resulting in varying microphysical characteristics of the raindrop spectrum. Therefore,  
183 considering the unique conditions of the Qinghai-Tibet Plateau, the rain intensity calculated based on  
184 the raindrop spectrum was categorized into five grades for calculation and analysis, as presented in  
185 Table 2. The samples from the four stations in the range of 0.5–5 mm·h<sup>-1</sup> were the largest, and the  
186 obtained standard deviation values were all very small. This indicates a high consistency in rain  
187 intensity distribution under weak rain intensity. In the interval of precipitation intensity greater than 20  
188 mm h<sup>-1</sup>, only two stations have samples, and one of the stations exhibits a large standard deviation.  
189 This reflects a significant inversion error in raindrop spectrum for Nyalam during short-duration heavy  
190 precipitation.

删除[远愚 段]: The results indicated that the mean value and standard deviation of the rain intensity at the same station were generally proportional to the rain intensity, with slight fluctuations observed among individual stations. The samples from the four stations in the range of 0.5–5 mm·h<sup>-1</sup> were the largest, and the obtained standard deviation values were all very small. This indicates a high consistency in rain intensity distribution under weak rain intensity

191 **Table 2: Descriptive statistics of rainfall intensity at the four stations.**

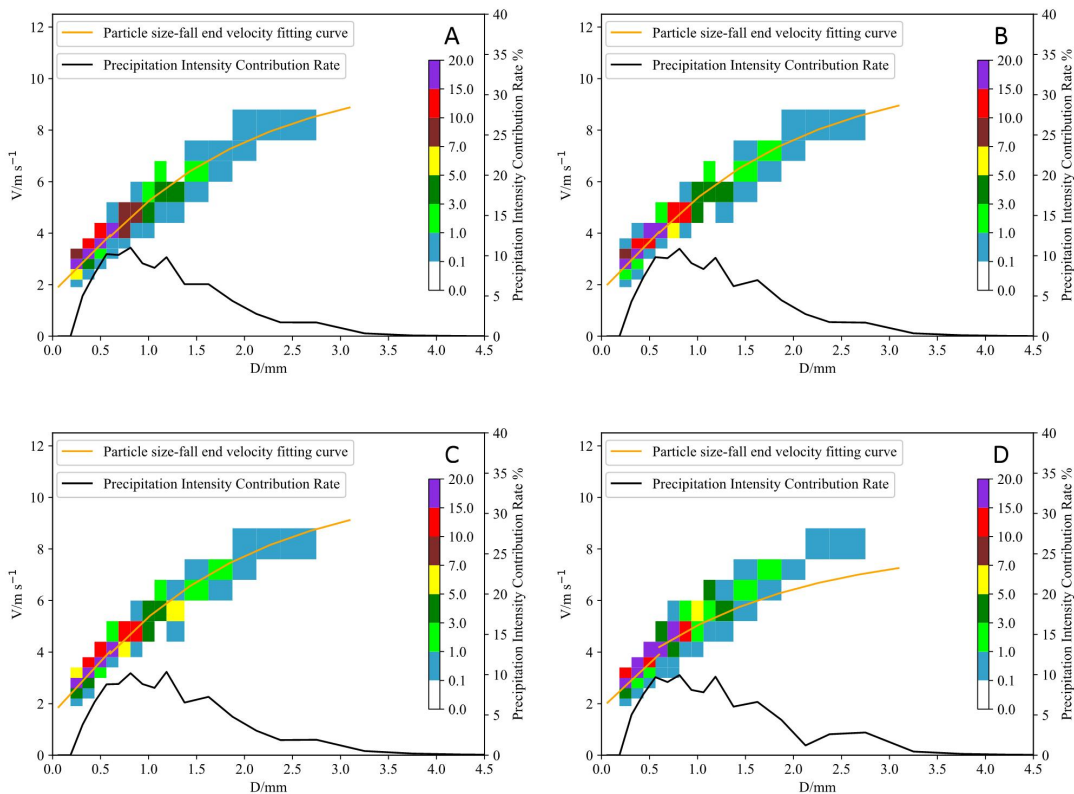
	Range (mm·h <sup>-1</sup> )	Sample Size	Mean (mm·h <sup>-1</sup> )	Standard Deviation	Precipitation (mm)
Nyalam	0.5–5	4047	2.16	1.21	146
	5–10	1358	7.38	1.28	166.6
	10–15	900	12.14	1.32	182.1
	15–20	656	17.69	1.37	193.4
	>20	960	30.63	7.99	490
Lhasa	0.5–5	3245	1.8	0.94	97.4
	5–10	180	5.87	0.77	17.6
	10–15	50	12.1	0	12.1
	15–20	0	0	0	0
	>20	0	0	0	0
Shigatse	0.5–5	7094	1.78	1.06	210.7
	5–10	584	6.37	1.11	62.02
	10–15	60	10.01	0	10.01



	15–20	0	0	0	0
	>20	0	0	0	0
	0.5–5	2389	3.27	1.5	130.1
	5–10	675	7.76	1.1	87.3
Naqu	10–15	479	13.73	1.21	109.6
	15–20	372	19.65	1.4	121.8
	>20	120	21.6	1.5	43.2

192 **3.1. Precipitation particle size, speed and rainfall intensity contribution rate distribution**

193 Figure 2 represent the mean precipitation values across the four stations. The canvas is divided into  
194 several rectangular areas defined by the coordinates of the horizontal and left axes, and the color code  
195 is applied to them. Each rectangular area represents a specific particle diameter and velocity. Figure 2  
196 reveals that the fitting curves of particle diameter distribution and terminal velocity at the four stations  
197 are approximately identical, and the terminal velocity increases with the particle diameter. Regarding  
198 particle number density, it is concentrated in the area with particle size less than 1 mm, and it decreases  
199 with the increase of diameter. Concerning the contribution rate of precipitation intensity, the four  
200 stations exhibit a multi-peak distribution, with peak diameters at 0.812 mm and 1.375 mm. In  
201 comparison with the precipitation process of convective clouds at low-altitude stations, the particle  
202 size spectrum width at the four stations on the Tibetan Plateau in this analysis was notably reduced, and  
203 the particle number density at the four stations with particle sizes greater than 3 mm was very low.



204  
205 **Figure 2: The average spectrum of precipitation particle size, velocity, and contribution rate distribution of**  
206 **precipitation intensity. The color bar represents the number density in units per m3. (A. Nyalam, B. Lhasa,**  
207 **C. Shigatse, and D. Naqu).**

208 Figure 3 displays the fitting relationship between the particle size of the raindrop spectrum and the  
209 terminal speed at the four stations in Tibet. For particle sizes less than 1.5 mm, the particle size at the  
210 four stations essentially aligns with the final terminal speed. For particle sizes greater than 1.5 mm, the  
211 speed is largest for Nyalam, followed by Naqu, and Lhasa has the smallest speed. However, under the  
212 same size, the final velocities of particles at the four stations are greater than those in Guizhou,  
213 exceeding 2 m/s. This may be attributed to the higher altitude of the four stations, which are over 3000  
214 m above sea level. This indicates that the high altitude of Tibet, due to thin air and low air pressure,  
215 results in decreased fall speed of larger particles of the same size. However, particles at lower altitudes  
216 (Shigatse and Lhasa) exhibited slightly Lower speeds than those at higher altitudes (Nyalam and Naqu).  
217 The fitting formulas for the v–D relationships at the four sites (Nyalam, Lhasa, Shigatse, and Naqu) are  
218 given by Equations 12, 13, 14, and 15, respectively. Considering the effect of air density on the fall  
219 velocity of raindrops as per Atlas et al. (1973), the correction factor  $(\rho_0/\rho)^{0.4}$  is multiplied to Equations  
220 12, 13, 14, and 15, resulting in the fitting relationship curves between the particle size of the raindrop  
221 spectrum and the terminal speed at the four stations in Tibet shown in Figure 3. The correction factor

删除[远愚 段]: Figure 3 displays the fitting relationship between the particle size of the raindrop spectrum and the falling speed at the four stations in Tibet. For particle sizes less than 1.5 mm, the particle size at the four stations essentially aligns with the final falling speed. For particle sizes greater than 1.5 mm, the speed is largest for Shigatse, followed by Lhasa, and Naqu has the smallest speed. However, under the same size, the final velocities of particles at the four stations are greater than those in Guizhou, exceeding 2 m/s. This may be attributed to the higher altitude of the four stations, which are over 3000 m above sea level. This indicates that the high altitude of Tibet, due to thin air and low air pressure, results in decreased fall speed of larger particles of the same size. However, particles at lower altitudes (Shigatse and Lhasa) exhibited slightly higher speeds than those at higher altitudes (Nyalam and Naqu). The fitting formulas for the v–D relationships at the four sites (Nyalam, Lhasa, Shigatse, and Naqu) are given by Equations 12, 13, 14, and 15, respectively.

222 for fall velocity considering air density is shown in Table 3.

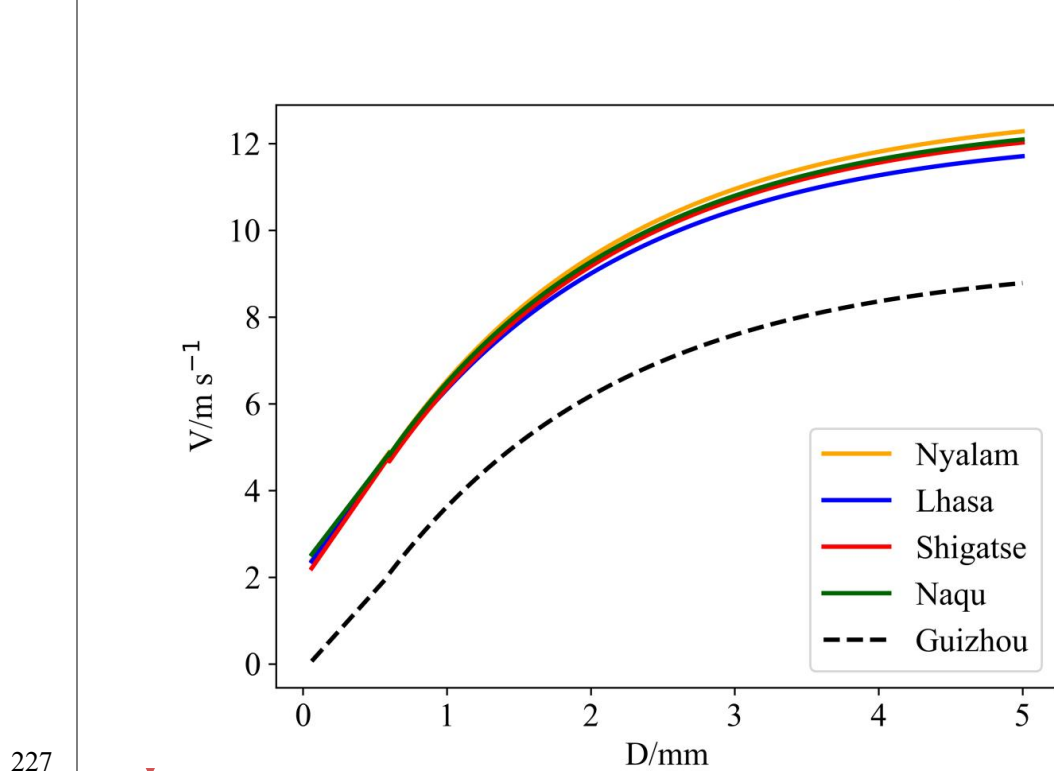
$$\begin{cases} v=0, & x < 0.03 \\ v = 3.720 \times (x+0.456), & 0.03 \leq x \leq 0.6 \\ v = 10.325 - 9.252 \times e^{-0.6x}, & x > 0.6 \end{cases} \quad (12)$$

删除[远愚 段]:

$$\begin{cases} v=0, & x < 0.03 \\ v = 3.796 \times (x+0.468), & 0.03 \leq x \leq 0.6 \\ v = 10.375 - 9.118 \times e^{-0.6x}, & x > 0.6 \end{cases} \quad (13)$$

$$\begin{cases} v=0, & x < 0.03 \\ v = 4.035 \times (x+0.401), & 0.03 \leq x \leq 0.6 \\ v = 10.614 - 9.568 \times e^{-0.6x}, & x > 0.6 \end{cases} \quad (14)$$

$$\begin{cases} v=0, & x < 0.03 \\ v = 3.474 \times (x+0.524), & 0.03 \leq x \leq 0.6 \\ v = 10.162 - 9.018 \times e^{-0.6x}, & x > 0.6 \end{cases} \quad (15)$$



227  
228 **Figure 3: The relationship between particle size and speed at four stations.**

229 **Table 3: The correction factor for fall velocity considering air density**

Correction factor $((\rho_0/\rho)^{0.4})$			
Nyalam	Lhasa	Shigatse	Naqu
1.240	1.179	1.185	1.240

230 设置格式[远愚 段]: 正文

231 The proportion of particle number density in raindrop spectrum and the contribution rate of  
232 precipitation are shown in Table 3 and Table 4, respectively.

233 **Table 4: Percentage of particle number density.**

删除[远愚 段]: 3

	Particle diameter (mm)		
	0-1 mm	1-2 mm	2-3 mm
Nyalam	93.60	6.15	0.25
Lhasa	92.41	7.24	0.35
Shigatse	91.45	8.06	0.49
Naqu	91.89	7.52	0.59

234 **Table 5: Percentage of precipitation contribution rate.**

删除[远愚 段]: 4

	Particle diameter (mm)		
	0-1 mm	1-2 mm	2-3 mm
Nyalam	55.63	37.32	7.05
Lhasa	54.60	38.16	7.24
Shigatse	51.12	40.49	8.39
Naqu	54.06	37.81	8.13

235 It can be observed from Table 3 that the number of precipitation particles with a distribution of 0-1 mm  
236 constitutes the largest proportion, exceeding 91%, while the proportion of particles with a distribution  
237 of more than 3 mm is comparatively smaller, being less than 0.6%. The proportion of precipitation  
238 intensity below 1 mm constitutes over 51%, with other particles comprising less than 49%. The results  
239 indicate that the contribution of precipitation intensity on the Tibetan Plateau is primarily concentrated  
240 in small particles with a diameter less than 1 mm.

241 In contrast to the convective cloud precipitation in Zheng'an, Guizhou analyzed by Wang(Wang et al.,  
242 2020), where convective cloud particles less than 1 mm account for 64.4%, the contribution rate to  
243 precipitation is only 17%; Additionally, it significantly differs from the rainstorm in Hainan analyzed  
244 by Mao(Mao et al., 2020). Despite the proportion of less than 1mm being 82.7%, the contribution rate  
245 is only 18.2%, and the rainstorm particle size spectrum in Hainan is remarkably wide. It is evident that  
246 the precipitation characteristics of convective clouds on the Qinghai-Tibet Plateau exhibit a  
247 particularity, wherein the diameter of precipitation particles is generally small, and the precipitation of

248 small-diameter particles constitutes a substantial proportion of the total precipitation.

### 249 3.2. Microphysical characteristic parameters of precipitation

250 The calculation of microphysical parameters based on raindrop spectra is divided into five levels  
251 according to different rainfall intensities. The mean diameter (Dm), average volume diameter (Dv),  
252 mode diameter (Dd), dominant diameter (Dp), and median diameter (Dnd) were calculated for four  
253 stations. Comprehensive analysis based on the characteristic parameters in Tables 6, 7, 8, and 9 shows  
254 that, under the same rainfall intensity level, Dm decreases with increasing altitude. The Dm at the  
255 higher-altitude Naqu and Nyalam stations is smaller than at the lower-altitude Lhasa and Shigatse  
256 stations. Under the same rainfall intensity level, Dv increases with altitude, with the smallest value at  
257 the low-altitude Lhasa station and the largest at the high-altitude Naqu station. When the rainfall  
258 intensity is less than  $\text{mm}\cdot\text{h}^{-1}$ , Dd increases with altitude (except for the Nyalam station), with the  
259 largest value at the Naqu station and the smallest at the Lhasa station, with the Shigatse station in  
260 between. When the rainfall intensity is greater than  $10\text{mm}\cdot\text{h}^{-1}$ , Dd decreases with altitude, with the  
261 largest value at the Lhasa station and the smallest at the Nyalam station, with the Shigatse and Naqu  
262 stations in between. When the rainfall intensity is less than  $10\text{mm}\cdot\text{h}^{-1}$ , Dp does not show a significant  
263 difference with altitude under the same rainfall intensity level. However, when the rainfall intensity is  
264 greater than  $10\text{mm}\cdot\text{h}^{-1}$ , Dp increases with altitude under the same rainfall intensity level (except for  
265 the Nyalam station). For the lower-altitude Lhasa and Shigatse stations, there is no significant  
266 difference in parameters under the same rainfall intensity. In contrast, for the higher-altitude Naqu and  
267 Nyalam stations, there are relatively obvious differences in parameters under the same rainfall intensity,  
268 with the Nyalam station's values being significantly smaller than those of the Naqu station. The reason  
269 for the smaller values at the Nyalam station compared to the nearby altitude Naqu station might be due  
270 to its unique geographical conditions. The above analysis indicates a strong correlation between  
271 altitude and these microphysical parameters. Dm shows a negative correlation with altitude under the  
272 same rainfall intensity, while Dv shows a positive correlation with altitude. For Dd and Dp, using  $10$   
273  $\text{mm}\cdot\text{h}^{-1}$  as the dividing line, there are different correlations with altitude under the same rainfall  
274 intensity level. Additionally, when the altitude is below 4000 m, there is no significant difference in  
275 characteristic diameters under the same rainfall intensity. Conversely, when the altitude is above 4000  
276 m, the differences in characteristic diameters become more pronounced.

删除[远愚 段]: Calculation of characteristic parameters such as mean diameter (Dm), average volume diameter (Dv), mode diameter (Dd), dominant diameter (Dp), and median diameter (Dnd) was conducted. Based on the comprehensive analysis of the characteristic parameters in Table 5, the Dm size at Lh. ...

删除[远愚 段]:

**Table 5: Microphysical parameters at the four stations.**

Station
Dm
Dv

...

277

**Table 6: Microphysical parameters of the Lhasa station.**

	<u>Range</u> (mm·h <sup>-1</sup> )	<u>Dm</u>	<u>Dv</u>	<u>Dd</u>	<u>Dp</u>	<u>Dnd</u>
<u>Lhasa</u>	<u>0.5-5</u>	<u>0.636</u>	<u>1.744</u>	<u>0.470</u>	<u>1.277</u>	<u>1.105</u>
	<u>5-10</u>	<u>0.809</u>	<u>2.058</u>	<u>0.671</u>	<u>1.869</u>	<u>1.628</u>
	<u>10-15</u>	<u>0.981</u>	<u>2.231</u>	<u>1.096</u>	<u>2.229</u>	<u>2.058</u>
	<u>15-20</u>	<u>1.008</u>	<u>2.288</u>	<u>1.069</u>	<u>2.256</u>	<u>2.095</u>
	<u>&gt;20</u>	<u>1.063</u>	<u>2.421</u>	<u>1.331</u>	<u>2.744</u>	<u>2.580</u>

278

**Table 7: Microphysical parameters of the Shigatse station.**

	<u>Range</u> (mm·h <sup>-1</sup> )	<u>Dm</u>	<u>Dv</u>	<u>Dd</u>	<u>Dp</u>	<u>Dnd</u>
<u>Shigatse</u>	<u>0.5-5</u>	<u>0.641</u>	<u>1.748</u>	<u>0.473</u>	<u>1.291</u>	<u>1.126</u>
	<u>5-10</u>	<u>0.815</u>	<u>2.044</u>	<u>0.685</u>	<u>1.901</u>	<u>1.639</u>
	<u>10-15</u>	<u>0.970</u>	<u>2.216</u>	<u>1.041</u>	<u>2.293</u>	<u>2.088</u>
	<u>15-20</u>	<u>1.000</u>	<u>2.298</u>	<u>1.277</u>	<u>2.612</u>	<u>2.292</u>
	<u>&gt;20</u>	<u>1.045</u>	<u>2.409</u>	<u>1.200</u>	<u>2.833</u>	<u>2.566</u>

279

**Table 8: Microphysical parameters of the Nyalam station.**

	<u>Range</u> (mm·h <sup>-1</sup> )	<u>Dm</u>	<u>Dv</u>	<u>Dd</u>	<u>Dp</u>	<u>Dnd</u>
<u>Nyalam</u>	<u>0.5-5</u>	<u>0.593</u>	<u>1.764</u>	<u>0.415</u>	<u>1.282</u>	<u>1.088</u>
	<u>5-10</u>	<u>0.725</u>	<u>2.064</u>	<u>0.498</u>	<u>1.865</u>	<u>1.574</u>
	<u>10-15</u>	<u>0.823</u>	<u>2.163</u>	<u>0.601</u>	<u>2.062</u>	<u>1.720</u>
	<u>15-20</u>	<u>0.905</u>	<u>2.217</u>	<u>0.846</u>	<u>2.351</u>	<u>2.022</u>
	<u>&gt;20</u>	<u>0</u>	<u>0</u>	<u>0</u>	<u>0</u>	<u>0</u>

280

**Table 9: Microphysical parameters of the Naqu station.**

	<u>Range</u> (mm·h <sup>-1</sup> )	<u>Dm</u>	<u>Dv</u>	<u>Dd</u>	<u>Dp</u>	<u>Dnd</u>
<u>Naqu</u>	<u>0.5-5</u>	<u>0.621</u>	<u>1.758</u>	<u>0.491</u>	<u>1.268</u>	<u>1.110</u>
	<u>5-10</u>	<u>0.808</u>	<u>2.071</u>	<u>0.777</u>	<u>1.730</u>	<u>2.022</u>

<u>10-15</u>	<u>0.922</u>	<u>2.250</u>	<u>0.947</u>	<u>2.434</u>	<u>2.205</u>
<u>15-20</u>	<u>0.970</u>	<u>2.313</u>	<u>1.005</u>	<u>2.595</u>	<u>2.291</u>
<u>&gt;20</u>	<u>1.043</u>	<u>2.479</u>	<u>1.166</u>	<u>3.004</u>	<u>2.673</u>

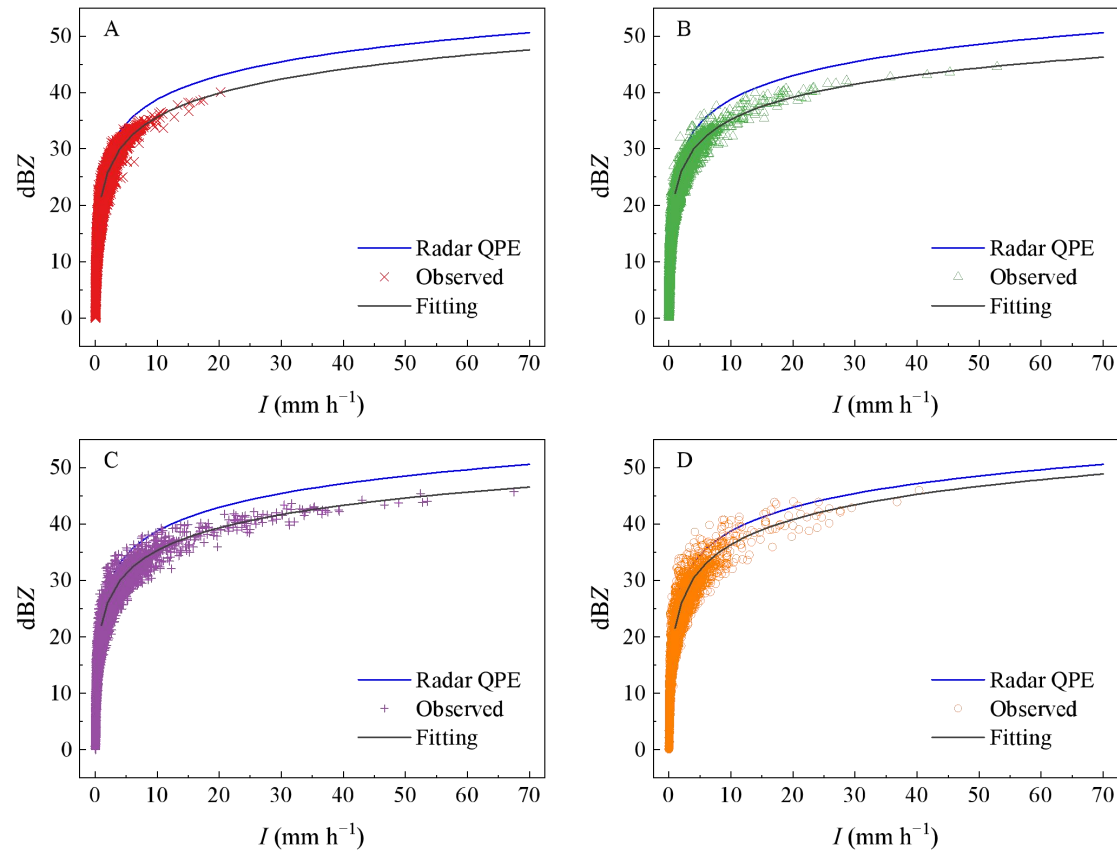
← 设置格式[远愚 段]: 正文

281

### 282 3.3. Z-I relation distribution

283 Utilizing Formulae (6) and (7), the radar reflectivity (Z) and precipitation intensity (I) are calculated

284 independently, and the data undergo fitting. The results are depicted in Figure 4.



285

286 **Figure 4: The Z-I relationships at four stations. (A. Nyalam, B. Lhasa, C. Shigatse, and D. Naqu)**

287 Figure 4 reveals that the suggested reference relation  $Z=300 \times I^{1.4}$  inaccurately predicts precipitation,

← 设置格式[远愚 段]: 上标

288 leading to an underestimation of precipitation intensity under identical radar reflectivity. With identical

289 radar reflectance, the precipitation intensity is highest in Lhasa, followed by Shigatse, while the

290 smallest precipitation intensity was observed in Naqu.

291 Table 6 shows the results of fitted Z-I relationships. Analyzing the altitude based differences in the Z-I

292 relationship, the a and b coefficients are similar for the station at 3653 m (Lhasa) and the station at

293 3910 m (Shigatse), while a and b for the station at 4519 m (Nyalam) and the station at 4560 m (Naqu)

294 are close. This observation indicates that the fitting parameter a is notably smaller, and the fitting  
 295 parameter b is larger for stations at higher altitudes.

296 **Table 10: Z-I relationship fitting results.**

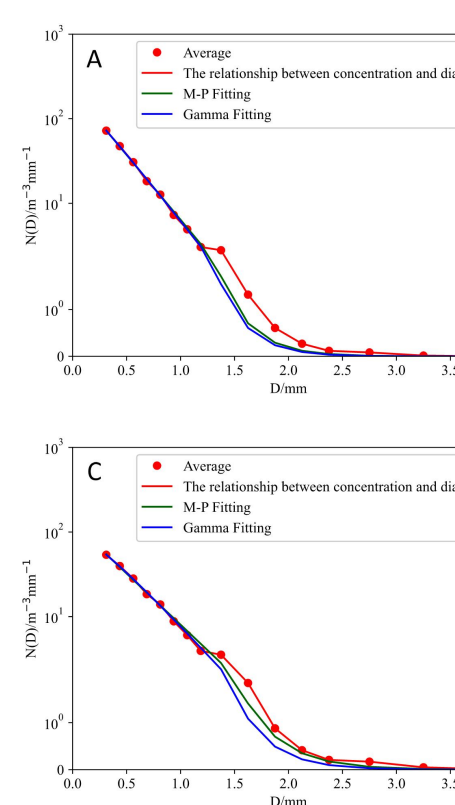
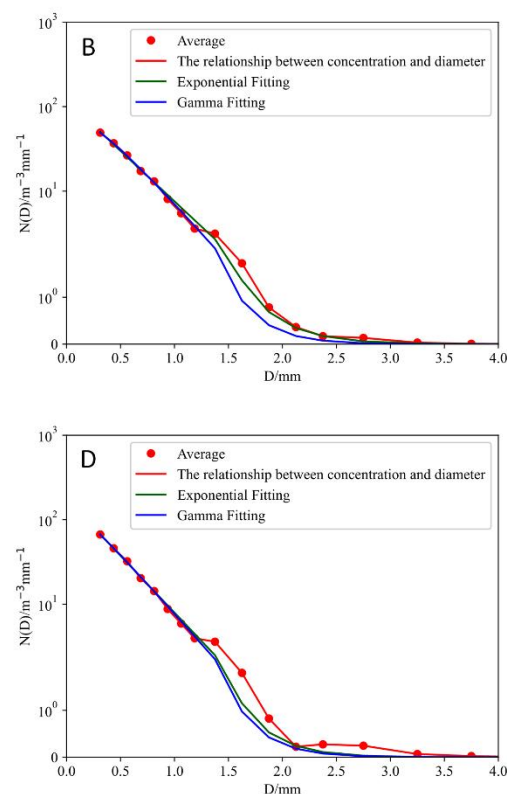
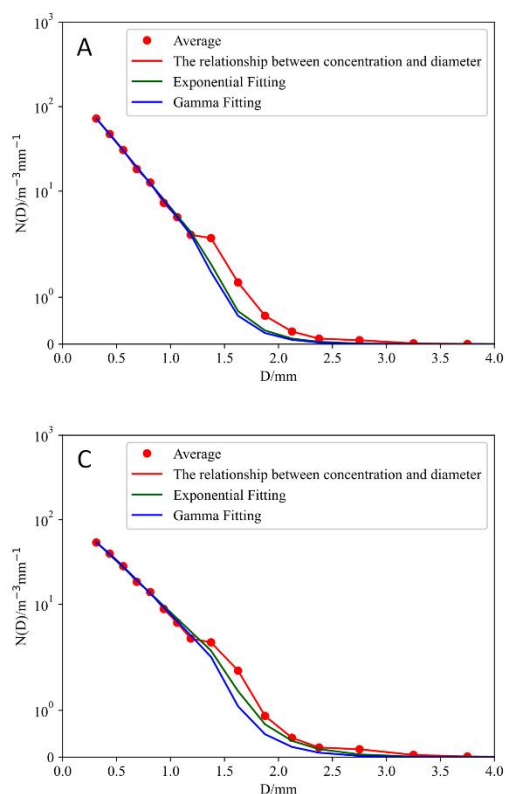
		$Z = aI^b$	
		Fitting	
		a	b
Nyalam	$Z=143.01 \times I^{1.41}$	143.01	1.41
Lhasa	$Z=162.56 \times I^{1.31}$	162.56	1.31
Shigatse	$Z=160.21 \times I^{1.33}$	160.21	1.33
Naqu	$Z=143.81 \times I^{1.48}$	143.81	1.48

删除[远愚 段]: 6

### 297 3.4. Precipitation particle distribution fitting

298 According to Formulas (8) and (9), the least squares method is applied to fit the Exponential and  
 299 Gamma distributions of the mean raindrop spectrum of precipitation at the four stations. The results are  
 300 presented in Figure 5 and Table 7.

删除[远愚 段]: M-P



301  
 302 **Figure 5: Exponential and Gamma intriptions for precipitation (A. Nyalam, B. Lhasa, C. Shigatse, and D.**  
 303 **Naqu).**

删除[远愚 段]:

删除[远愚 段]: M-P

304 As indicated in Table 7,  $\mu$  decreases with increasing altitude in the Gamma distribution. A smaller  $\mu$



305 corresponds to a wider raindrop spectrum, signifying that the diameter of raindrops increases with  
306 altitude. The raindrop mean diameter at higher altitudes is larger, corresponding to the precipitation  
307 microphysical characteristics calculated in Table 5. Conversely, the fitting results of the Exponential  
308 distribution show that  $N_0$  and  $\lambda$  exhibit a clear increasing trend with height. In Figure 5, the abscissa  
309 represents particle diameter, and the ordinate represents particle number density. The curve trends at the  
310 four stations are relatively consistent. For Nyalam station, the Exponential distribution is given by  
311  $N(D)=218.78 \times e^{-3.53D}$ , and the Gamma distribution is  $N(D)=282.14 \times D^{0.15} \times e^{-3.82D}$ . For Lhasa  
312 station, the Exponential distribution is  $N(D)=118.70 \times e^{-2.75D}$ , and the Gamma distribution is  
313  $N(D)=250.40 \times D^{0.43} \times e^{-3.56D}$ . For Shigatse station, the Exponential distribution is  
314  $N(D)=130.35 \times e^{-2.79D}$ , and the Gamma distribution is  $N(D)=216.08 \times D^{0.29} \times e^{-3.35D}$ . Finally, for  
315 Naqu station, the Exponential distribution is  $N(D)=177.22 \times e^{-3.10D}$ , and the Gamma distribution is  
316  $N(D)=238.95 \times D^{0.17} \times e^{-3.44D}$ . In the Gamma distribution, two parameters,  $\mu$  and  $\lambda$ , represent the  
317 curve shape factor and particle scale parameters, respectively, as shown in Equation (9). According to  
318 Equation (10), the two parameters  $\mu$  and  $\lambda$  for the four stations are fitted with an analytical binomial  
319 relationship, and the coefficients are presented in Table 8.

320 **Table 11: Gamma fitting and Exponential fitting results.**

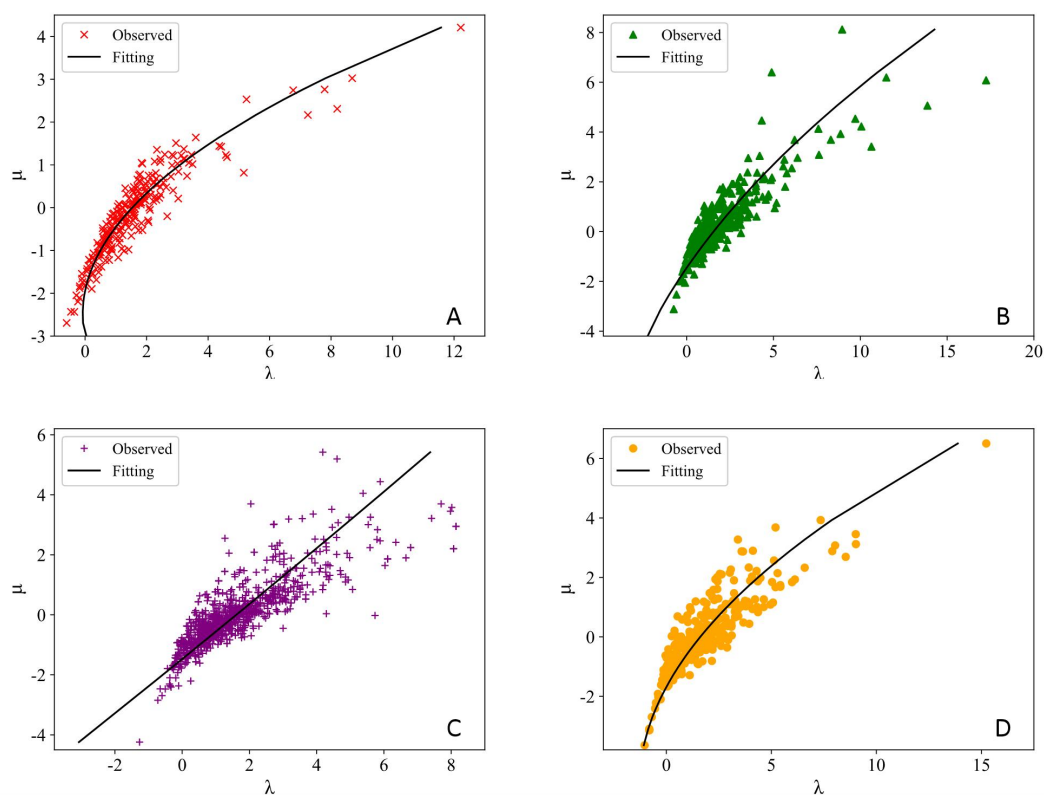
	Gamma			<u>Exponential</u>	
	$N_0$	$\mu$	$\lambda$	$N_0$	$\lambda$
Nyalam	284.90	0.15	3.83	218.93	3.53
Lhasa	253.26	0.44	3.59	118.81	2.75
Shigatse	217.69	0.30	3.35	130.45	2.79
Naqu	240.91	0.18	3.45	177.34	3.10

321 **Table 12:  $\mu$  and  $\lambda$  binomial parameters**

	$\lambda = a\mu^2 + b\mu + c$		
	$a$	$b$	$c$
Nyalam	0.2816	1.2798	1.5074
Lhasa	0.1717	1.0589	1.3983
Shigatse	0.0221	1.1215	1.6002
Naqu	0.0155	1.2141	1.7599

322 It can be observed from Figure 6 that, although the four curves bend towards the lambda axis, the  
323 degree of bending varies. The curves for Shigatse exhibit nearly straight curves, whereas the curves for  
324 Nyalam and Naqu are more pronounced in their curvature towards the lambda axis. The  $\mu$ - $\lambda$   
325 relationship varies among the four stations, and this variation is associated with the mass-weighted

326 diameter. Eq. (11) indicates that when  $\lambda$  remains constant, a higher  $\mu$  value corresponds to a greater  
327 mass-weighted average diameter.



328  
329 **Figure 6:  $\mu$ - $\lambda$  relationship (A. Nyalam, B. Lhasa, C. Shigatse, D. Naqu).**

#### 330 4. Conclusions

331 In this study, we conducted a statistical analysis of raindrop spectrum data above light and moderate  
332 rain at four sites in Tibet, considering different heights, latitudes, and longitudes. The analysis includes  
333 precipitation particle size distribution, particle landing speed, precipitation particle number density, and  
334 rainfall intensity at the end. Additionally, the relationship between Z-I distribution and rainfall rate,  
335 precipitation particle distribution fitting, and analysis of Gamma distribution  $\mu$ - $\lambda$  parameters for the  
336 precipitation raindrop spectrum characteristics at the four stations are examined. A comparison is made  
337 between the data from the four stations on the Qinghai-Tibet Plateau and some non-plateau areas.  
338 Simultaneously, the analysis of raindrop spectrum data at the Naqu station reveals certain similarities  
339 with previous studies (indicating convective cloud as the primary precipitation at Naqu station).  
340 However, some differences are noted, such as the mean spectral width of convective precipitation at the  
341 Naqu station being relatively narrow.

342 The relationship between precipitation particle size and particle landing velocity at the four stations  
343 indicates that the terminal velocity of the four stations essentially coincided when the particle size was  
344 less than 1.5 mm. For particle sizes greater than 1.5 mm, the terminal velocity of particles at the four  
345 stations is faster at high altitudes than at medium and low altitudes. At the four stations, the proportion  
346 of precipitation raindrop spectral particle size less than 1 mm exceeded 91%, and the contribution rate  
347 of precipitation was more than 51%. The characteristics of convective cloud precipitation over the  
348 Tibetan Plateau exhibit peculiarities that differ from the raindrop spectrum characteristics in the  
349 low-altitude areas of the mainland.

删除[远愚 段]: the terminal velocity of particles at the four stations is faster at medium and low altitudes than at high altitudes.

删除[远愚 段]: This is attributed to instruments at high altitudes being closer to the clouds.

350 The six microphysical characteristics at the four stations have different correlation relationships with  
351 altitude under different rainfall intensities. Dm exhibits a negative correlation with altitude at the same  
352 rainfall intensity; in contrast, Dv shows a positive correlation with altitude. For microphysical  
353 parameters such as Dd and Dp, a rainfall intensity of 10 mm·h<sup>-1</sup> serves as the boundary line, and they  
354 have different correlation relationships with altitude under the same rainfall intensity level. Regarding  
355 the fitted Z-I relationship, the fitting parameter a at the high-altitude station is significantly smaller,  
356 while the fitting parameter b is larger. The particle spectrum of high-altitude stations is broader, with a  
357 larger equivalent diameter, and the reflectivity of high-altitude stations is significantly higher than that  
358 of low-altitude stations.

删除[远愚 段]: The six microphysical characteristic parameters at the four stations all increased with altitude, showing a positive correlation with altitude. Regarding the fitted Z-I relationship, the fitting parameter a at the high-altitude station is significantly smaller, while the fitting parameter b is larger. The particle spectrum of high-altitude stations is broader, with a larger equivalent diameter, and the reflectivity of high-altitude stations is significantly higher than that of low-altitude stations.

359 The concentration of small raindrops (less than 1 mm) in the raindrop spectrum of high-altitude  
360 stations on the Tibetan Plateau was higher. Both the Exponential distribution and the Gamma  
361 distribution exhibit good fitting effects for low-altitude stations. Overall, the Exponential fit slightly  
362 better. In the relationship between the  $\mu$  and  $\lambda$  of the two parameters in the Gamma distribution, the  
363 larger the  $\mu$ , the larger the weighted average diameter of the mass when the  $\lambda$  remains constant. In other  
364 words, the greater the  $\mu$ , the greater the precipitation intensity when  $\lambda$  remains unchanged.

删除[远愚 段]:

删除[远愚 段]: M-P

删除[远愚 段]: M-P

删除[远愚 段]: performed

### 365 Data Availability Statement

366 The data used to support the findings of this study are available from the corresponding author upon  
367 request.

368 **Author Contributions**

369 Conceptualization, F.W. and G.C.; methodology, F.W. and Q.W.; software, Y.H.,Y.D and Q.W.;  
370 writing—review and editing, F.W., Y.H. ,Y.D and Y.C.; resources,T.Z. and J.L.; supervision, T.Z. and  
371 G.C. All authors have read and agreed to the published version of the manuscript.

372 **Competing interests**

373 The contact author has declared that none of the authors has any competing interests.

374 **Disclaimer**

375 Publisher’s note: Copernicus Publications remains neutral with regard to jurisdictional claims made in  
376 the text, published maps, institutional affiliations, or any other geographical representation in this paper.  
377 While Copernicus Publications makes every effort to include appropriate place names, the final  
378 responsibility lies with the authors.

379 **Acknowledgements**

380 We thank the Tibet Meteorological Bureau for the raindrop spectrum data, and the students and  
381 teachers of Chengdu University of Information Technology for their help.

382 **Financial support**

383 This research was funded by the Open Fund project for Key Laboratory of Land Surface Process and  
384 Climate Change in Cold and Arid Regions, Chinese Academy of Sciences (LPCC2020009), and the  
385 Natural Science Foundation of Sichuan Province (2022NSFSC0208) and National Natural Science  
386 Foundation of China (42075001).

387 **References**

388 Atlas, D., Srivastava, R. C., and Sekhon, R. S.: Doppler characteristics of precipitation at vertical  
389 incidence, *Rev. Geophys*, 1973, 11, 1-35, doi:10.1029/RG011i001p00001, 1973.  
390 Battaglia, A., Rustemeier, E., Tokay, A., Blahak, U., and Simmer, C: PARSIVEL snow observations: A

391 critical assessment, *J. Atmos. Ocean. Tech*, 27, 333-344, doi: 10.1175/2009JTECHA1332.1, 2010.

392 Chang, Y., and Guo, X. L.: Characteristics of convective cloud and precipitation during summer time at  
393 Nagqu over Tibetan Plateau, *Sci. Bull*, 61, 1706–1720, doi:10.1360/N972015-01292, 2016.

394 Carlton, W. U., and David, A.: Assessment of the contribution of differential polarization to improved  
395 rainfall measurements, *Radio Science*, 19, 49-57, doi:10.1029/RS019i001p00049, 1984.

396 Jiang, J. X., and Fan, M. Z.: Convective clouds and mesoscale convective systems over the Tibetan  
397 Plateau in summer, *Chin. J. Atmos. Sci*, 26, 263-270, doi:10.3878/j.issn.1006-9895.2002.02.12, 2002.

398 Kruger, A., and Krajewski, W. F.: Two-Dimensional Video Disdrometer: A Description, *J. Atmos.*  
399 *Ocean. Tech*, 19, 602-617, doi:10.1175/1520-0426(2002)019<0602:TDVDAD>2.0.CO, 2002.

400 Li, D., Bai, A. J., Xue, Y. J., and Wang, P.: Comparative analysis on characteristics of summer  
401 convective precipitation over Ti-betan Plateau and Sichuan Basin, *Meteor. Mon.*, 40, 280-289, doi:  
402 10.7519/j.issn.1000-0526.2014.03.003, 2014.

403 Li, L. G., and De, L. G. E.: Analyses of microphysical features for spring precipitation cloud layers in  
404 east of Qinghai, *Plateau Meteorology*, 20, 191-196, doi:10.3321/j.issn:1000-0534.2001.02.013, 2001.

405 Liu, L. P., Zheng, J. F., Ruan, Z., Cui, Z. H., Hu, Z. Q., Wu, S. H., et al.: The preliminary analyses of  
406 the cloud properties over the Tibetan Plateau from the field experiments in clouds precipitation with the  
407 various radars, *Acta. Meteor. Sin*, 73, 635-647, doi:10.11676/qxxb2015.041, 2015.

408 Li, S. S., Wang, X. F., Wan, R., and Li, G. P.: The Characteristics of Raindrop Spectrum in Different  
409 Altitude Region on the Eastern Slope of Qinghai-Xizang Plateau, *Plateau Meteorology*, 39, 899-911,  
410 doi:10.7522/j.issn.1000-0534.2019.00086, 2020.

411 Marshall, J. S., and Palmer, W. M.: The Distribution of Raindrops with Size, *J. Meteor*, 5, 165-166,  
412 doi: 10.1175/1520-0469(1948)005<0165:TDORWS>2.0.CO;1948

413 Mao, Z. Y., Huang, G. R., Huang, Y. B., Li, G. W., and Xing, F. H.: Characteristics Analysis of  
414 Raindrop Size Distribution during Hainan Autumn-Rainstorm Process, *Natural Science Journal of*  
415 *Hainan University*, 38, 59-66, doi:10.15886/j.cnki.hdxzbzkb.2020.0009, 2020.

416 Ruan, Z., Jin, L., Ge, R. S., Li, F., and Wu, J.: The C-band FMCW pointing weather radar system and  
417 its observation experiment, *Acta. Meteor. Sin*, 3, 577-592, doi:10.11676/qxxb2015.039, 2015.

418 Shu, L., Li, M. S., Hua, S., Suo, L. J. C., Lv, Z., Fu, W., et al.: Statistical Characteristics of Raindrop  
419 Size Distribution and Microphysical Structure of Cloud in Yushu Region of Qinghai Tibet Plateau,  
420 *Advances in Meteorological Science and Technology*, 11, 113-121+134,

421 doi:10.3969/j.issn.2095-1973.2021.04.016, 2021.

422 Shi, J. S., Zhang, W., Chen, T. Y., Bi, J. R., and He, M.: Raindrop-size distribution characteristics of the  
423 northern face of Qilian Mountains in the summer of 2006, *J. Lanzhou University(Natural Sciences)*, 44,  
424 55-61, doi: 10.3321/j.issn:0455-2059.2008.04.011, 2008.

425 Ulbrich, C. W.: Natural Variations in the Analytical Form of the Raindrop Size Distribution, *J. Climate*.  
426 *Appl. Meteor*, 22, 1764-1775, doi:10.1175/1520-0450(1983)022<1764:NVITAF>2.0.CO;2, 1983.

427 Wang, F. Z., Wang, Q. S., He, S., Gu, X. P., and Yu, F.: Analysis of Summer Raindrop Spectrum  
428 Characteristics of Zheng'an in Guizhou, *J. Chengdu University. Inf Technology*, 35, 689-696,  
429 doi:10.16836/j.cnki.jcuit.2020.06.016, 2020.

430 Xu, X. D., and Chen, L. S.: Advances of study on Tibetan Plateau experiment of atmospheric sciences,  
431 *J. Appl. Meteor. Sci*, 17, 756-772, doi:10.3969/j.issn.1001-7313.2006.06.013, 2006

432 Xiong, J. N., Li, W., Liu, Z. Q., Cheng, W. M., Fan, C. K., and Zhang, H.: Monitoring and analysis of  
433 historical drought in southeast Tibet based on multi--source data, *Arid Land Geography*, 42, 735-744,  
434 doi:10.12118/j.issn.1000—6060.2019.04.04, 2019.

435 Yu, J. Y., Li, M. S., and Yin, S. C.: Analysis of Cloud Precipitation Microscopic Characteristic  
436 Raindrop Spectrum in Nagqu Area of Qinghai-Tibet Plateau, *J. Chengdu University. Inf Technology*, 35,  
437 188-194, doi:10.16836/j.cnki.jcuit.2020.02.010, 2020.

438 Zhang, N. J., Xiao, T. G., and Jia, L.: Spatial and Temporal Characteristics of Precipitation in the Tibet  
439 Plateau from 1979 to 2016, *J. Arid. Meteorology*, 36, 373-382,  
440 doi:10.11755/j.issn.1006-7639(2018)-03-0373, 2018.

441 Zhang, G., Vivekanandan, J., Brandes, E. A., Meneghini, R., and Kozu, T.: The Shape-Slope Relation  
442 in Observed Gamma Raindrop Size Distributions: Statistical Error or Useful Information?, *J. Atmos.*  
443 *Ocean. Tech*, 20, 1106-1119, doi:10.1175/1520-0426(2003)020<1106:TSRIOG>2.0.CO;2, 2003.